AEROGEL SUPPORTED COPPER NANOPARTICLES BY THE ADSORPTION OF A NEW COPPER CHELATE FROM SUPERCRITICAL CARBON DIOXIDE

Selmi Erim Bozbag[1], Svetlana O. Kostenko[2], Michael A. Kurykin[2], Viktor N. Khrustalev[2], Lichun Zhang[3], Mark Aindow[3] and Can Erkey[1,*]

[1] Deparment of Chemical and Biological Engineering, Koç University, 34450, Sariyer, Istanbul, TURKEY

[2]A.N. Nesmeyanov Institute of Organoelement Compounds, Russian Academy of Sciences, 19991, V-334, Moscow, RUSSIA.

[3] Department of Chemical, Materials and Biomolecular Engineering, Institute of Material Science, University of Connecticut, Storrs, CT 06269, USA.

ABSTRACT

In this study, we used supercritical deposition (SCD) method to incorporate of Cu, Cu_2O, CuO and $Cu@Cu_2O$ core-shell nanoparticles onto carbon (CA), resorcinol-formaldehyde (RFA) and silica aerogels (SA). We present a brand new polyfluorinated copper precursor. copper bis(1,1,1,3,5,5,6,6,6-nonafluorohexane-2,4-diiminate (CuDI6), which has a high solubility in supercritical carbon dioxide ($scCO_2$). Adsorption isotherms of CuDI6 onto various aerogels from $scCO_2$ were determined at 35°C and 10.6 MPa. The affinity between CuDI6 and different aerogels changed in the following order: CA>RFA>SA. The conversion of aerogel supported CuDI6 into nano sized copper species was carried out via a post adsorption sequence at low pressure involving N_2 and H_2 treatments at temperatures ranging from 200 to 300°C. The oxidation state (Cu, Cu_2O or CuO) and morphology (single particle, phase segregated or core-shell) of the supported nanoparticles were manipulated by changes in the post-adsorption sequence. The characterization of the materials was carried out using thermogravimetry (TGA), X-ray diffraction (XRD), and transmission electron microscope (TEM).

1. INTRODUCTION

Supported copper nanoparticles are of great interest in areas such as catalysis and microelectronics[1] due to their redox capacity, high electrical conductivity and low cost. These properties allow numerous catalytic applications including NO reduction [2], removal from gas exhausts[3], and methanol steam reforming[4] on organic supports.

Aerogels are nanostructured foams with tunable properties. They have attracted a great deal of interest in catalysis, in environmental and thermal engineering as well as in biotechnology. Carbon aerogels (CA) are produced by the pyrolysis of resorcinol-formaldehyde aerogels (RFA) which are synthesized by the supercritical drying of gels produced from the condensation polymerization of resorcinol and formaldehyde in an aqueous solution. Silica aerogels are also produced by the supercritical drying of gels formed by a hydrolysis and condensation reactions between a silica precursor and water. Aerogels are mesoporous materials with high surface areas, low densities and narrow pore size distributions. The properties such as pore size pore volume and density can be controlled by changing the reactant concentrations used in the sol-gel synthesis. CA and RFA supported copper are promising candidates as heterogeneous catalysts and sensors. SA supported Cu is a promising material as a catalyst and as a transparent conductor.

A promising technique to prepare aerogel composites is supercritical deposition (SCD) which is proven to be a very effective technique in the synthesis of supported highly dispersed nanoparticles[5, 6]. SCD consist of a series of steps including the dissolution of a metal precursor in a supercritical fluid, adsorption of the metal precursor from the fluid phase onto the surface of the support and finally the conversion of the metal precursor to its metal form by several techniques[7]. Carbon dioxide (CO_2) has been the most commonly used supercritical fluid (SCF) since it is non-toxic, non-flammable and inexpensive. Supercritical CO_2 (scCO2) has intermediate physical properties between gas and liquid. The gas-like diffusivity and viscosity of $scCO_2$ are favorable for rapid diffusion and permeation into porous substrates whereas the liquid-like density allows for the dissolution of a wide range of organometallic precursors. The low surface tension of $scCO_2$ provides better penetration and wetting of pores as compared to conventional liquid solvents. It also prevents pore collapse which may occur on fragile morphologies such aerogels when organic solvents are used. Furthermore, residual CO_2 is negligible in the processed product because of the gaseous character of CO_2 near ambient conditions. SCD have been used to incorporate metallic nanoparticles onto various types of substrates[6-11]. However, there is no study for the preparation aerogel supported Cu.

SCD necessitates the use of $scCO_2$ soluble metal precursors. Most of the metal precursors (including acetylacetonates and hexafluoroacetylacetonate) have rather limited solubility in $scCO_2$ ((2.2-5.7) x 10^{-3} mol/L at 40 °C and pressure ranging from 10.3 to 31 MPa)[12, 13]. This fact imposes to use of organic entrainers such as ethanol, methanol or isopropyl alcohol with dense CO_2 in order to dissolve aforementioned metal precursors [9, 14]. The use of such entrainers may create an extent of surface tension and may cause damage on the nanostructured pores of aerogels as previously mentioned.

An understanding of the thermodynamics for adsorption of the metal precursor onto the support material is crucial for the design of large scale SCD technology for synthesis of supported nanoparticles. Along that line, we recently proposed a measurement method for the adsorption of solutes from $scCO_2$ onto substrates based on the analysis of the fluid phase concentration[15]. We have shown that the aforementioned technique gives more realistic perspective on the adsorption of $Pt(cod)me_2$ on RFAs as compared to the gravimetric investigations carried out previously in the literature [15]. In the literature, there are a few papers which deal with the adsorption of metal precursors from $scCO_2$ onto a number of substrates [15-18]. However, there is not any systematic study on the effect of substrates which possess different surfaces chemistries on the adsorption isotherms. The effect of temperature on the adsorption of metal precursors from $scCO_2$ is not clear as well.

Therefore, in this work, we investigated the adsorption isotherms CuDI6 from $scCO_2$ onto a hydrophobic (CA & RFA), and hydrophilic (SA) substrates. We studied the adsorption isotherms of CuDI6-CO_2-CA system at different temperatures as well. Then the conversion of CuDI6 and the formation of Cu containing nanocrystals were investigated using TGA, XRD and TEM.

2. MATERIALS AND METHODS

2.1. Materials

Resorcinol (99 %), sodium carbonate (99.99 %) and ethanol (99.9 % purity) were purchased from Merck. Formaldehyde (36 %) was purchased from Lachema. The chemicals

were used as-received. Water was distilled and deionized. Carbon dioxide (99.998 %), hydrogen, nitrogen and synthetic air were purchased from Messer Aligaz.

2.2. Synthesis of Cu precursor

To a solution of $(CH_3COO)_2Cu$ (2.5 g) in distilled water (30 ml) was added a solution of 2-amino-4-iminoperfluorohex-2-ene (5.6 g) in $CHCl_3$ (20 ml). The reaction mixture was stirred for 30 min., the organic layer was separated and washed with water. The solvent was evaporated and the solid residue 5.8 g (90.8%) was pure copper bis(1,1,1,3,5,5,6,6,6-nonafluorohexane-2,4-diiminate) as green-brown crystals ($C_{12}H_4CuF_{18}N_4$, molecular weight = 609.73 g/mol). The melting point of the chemical is 113-114°C.

2.2. Synthesis of aerogels

RFAs were synthesized via the sol-gel route described by Pekala [19] which involves the polymerization of resorcinol (R) and formaldehyde (F) with an alkali catalyst (C) in water (W) followed by gelation and cross-linking periods. The gelation was carried out at ambient temperature for 1 day, followed by a curing sequence that comprised one day at 50°C and then three days at 90 °C. The initial molar ratios of R/F, R/C and R/W were 0.5, 200 and 0.02, respectively. Afterwards, the resulting hydrogel was placed in an acetone bath to replace the water in the pores with acetone. Finally, acetone was extracted from the gels using $scCO_2$ at 13.8 MPa and 50 °C. CAs were prepared via the pyrolysis of the RFAs at 1000 °C in N_2 flow (100 cm^3/min).

Silica aerogels used in this study were synthesized by a two-step procedure using TEOS as the precursor, HCl as the hydrolysis catalyst and NH_4OH as the condensation catalyst. A 50 wt. % solution of TEOS in ethanol was prepared. Subsequently, water and acid catalyst were added to start hydrolysis under continuous stirring. Condensation started with the addition of the base catalyst and the sol was taken into cylindrical molds with a diameter of 10mm. The overall mole ratio of TEOS to water was 1:4, HCl to TEOS was 500:1, and NH_4OH to TEOS was 80. These mole ratios were kept constant in the aerogel synthesis. After gelation, the alcogels were taken out from the mold and placed in an aging solution which was 50 vol. % ethanol and water, and left in a furnace at 323.2 K for 20 hours. The aim of the aging step was to improve the mechanical strength of the alcogels. After the aging step was completed, the aging solution was replaced with pure ethanol and the alcogels were kept for three more days in pure ethanol in order to displace all the water. In order to extract ethanol from the pores of the alcogel, drying with $scCO_2$ was used which was conducted at 313.2 K and 8.27 MPa. The cylindrical aerogels were then crushed into small particles of 2-4 mm for the adsorption equilibrium measurements.

2.3. SCD and precursor conversion

Supercritical deposition experiments and the equilibrium adsorption measurements were carried out in the experimental setup presented in Figure 2. The 57 mL stainless steel vessel was custom-made and equipped with two sapphire windows (2.5 cm in diameter (Sapphire Engineering, Inc., Pocasset; MA), a T-type thermocouple assembly (Omega Engineering), a pressure transducer (Omega Engineering), a vent line, and a rupture disk assembly (Autoclave Engineers). The vessel was sealed with poly(ether ether ketone) O-rings. For each experiment, a certain amount of CuDI6 was placed in the vessel along with a stirring bar, and a certain amount of aerogel (CA, RFA or SA) substrate. A stainless steel screen was placed in the middle of the vessel in order to separate the substrate and the stirring bar. The system was sealed and heated to the desired temperature by a circulating

heater/cooler (Cole Parmer, Model 12108-15). The system was pressurized with CO_2 using a syringe pump (ISCO, 260D) up to the desired pressure and kept at these conditions for the desired exposure time. During this process, CuDI6 dissolved in the $scCO_2$ and adsorbed onto the substrate from the fluid phase. After exposure, the system was depressurized slowly (0.7 MPa/min) using a needle valve (Autoclave Engineers), and the CuDI6/aerogel composite was removed from the vessel. Crushed aerogel particles were used for the equilibrium measurements.

The conversion of CuDI6 was investigated in atmospheric pressure at various temperatures in reacting (H_2) or inert gas (N_2) media. The composite was placed in a custom-made quartz process tube (internal diameter 3 cm, length 57 cm) in a tube furnace (model F1125 Thermolyne). The impregnated metal precursor was exposed to aforementioned gases at a temperature range of 160-300°C in flowing gas (100 cm^3/min) for 2 h. The system was cooled to room temperature under flowing N_2. The composite was then removed from the process tube and the metal loading was measured from the weight change using an analytical balance (AND GR-200, accurate to ±0.1 mg).

2.4. Adsorption measurements

The adsorbed amount of CuDI6 was determined by analyzing the concentration variation of CuDI6 in the fluid phase. The details of the procedure are given elsewhere [15]. The CuDI6 concentration in each of the samples was analyzed by HPLC using 100 % ethanol with a flow rate of 1 ml/min as the mobile phase and with the wavelength of the UV detector lamp set to 270 nm. This wavelength was selected based on the UV spectra of a CuDI6 in ethanol solution with a mass fraction of 100 ppm CuDI6/ethanol. A series of CuDI6-ethanol solutions with mass fractions ranging from (0 to 200 ppm) were used as the calibration solutions. Calibration curves were prepared and updated before every measurement sequence. The HPLC analyses were repeated twice and the mean of the two measurements were used. The isotherm measurements were duplicated twice. Isotherms for 3 different aerogels (CA, RFA and SA) were measured at 35 °C and 10.6 MPa.

2.5. Materials characterization

X-ray diffraction data of CuDI6 were collected on an automated four-circle Siemens P3/PC diffractometer (λ(MoK$_\alpha$)-radiation, graphite monochromator, $\omega/2\theta$ scan mode, θ_{max} = 28°) and corrected for absorption using the ψ-scan technique. The structure was solved by direct methods and refined by full-matrix least squares technique on F^2 with anisotropic displacement parameters for non-hydrogen atoms. The hydrogen atoms were localized in the difference-Fourier map and refined isotropically. The final divergence *R*-factors were R_1 = 0.033 for 1943 independent reflections with $I > 2\sigma(I)$ and wR_2 = 0.150 for all 2065 independent reflections, S=1.056. All calculations were carried out using the *SHELXTL* program. Crystallographic data for CuDI6 have been deposited with the Cambridge Crystallographic Data Center. CCDC 821069 contains the supplementary crystallographic data for this paper. These data can be obtained free of charge from the Director, CCDC, 12 Union Road, Cambridge CB2 1EZ, UK (Fax: +441223336033;e-mail: deposit@ccdc.cam.ac.uk or www.ccdc.cam.ac.uk). Mass-spectrum of CuDI6 was obtained using a VG 7070E spectrometer (70eV).

The pore size, pore volume and the Brunauer, Emmett and Teller (BET) surface area of aerogel samples were determined by nitrogen physisorption using a Micromeritics ASAP 2020 instrument. 60-point N_2 adsorption/desorption isotherms with a relative pressure (P/P0) ranging from 10^{-7} to 1 (which required at least 50 h of continuous operation) were obtained. The pore size distributions of these samples were determined using the Barrett, Joyner and

Halenda (BJH) method. The desorption branch of the isotherm was used for the pore size analysis since the desorption process is thermodynamically stable.

Decomposition of aerogel supported CuDI6 was followed via the IR spectra of the samples which were obtained using an Thermo Scientific Nicolet iS10 Smart iTR spectrometer. TG analyses of the samples were conducted in argon atmosphere at desired temperature programs using a Seiko Instruments SSC5200 TG-DT220 apparatus. XRD continuous measurements were carried out by using Cu Kα source Huber G 670 Imaging Plate in a 2θ range of 5^0- 87^0 with a scanning rate of 5.50^0 min^{-1}. The mean diameters of the Cu and Cu_2O nanoparticles were calculated from the full width at half maximum of the desired peak using the Scherrer formula. The morphology of the supported catalysts was characterized by high-resolution TEM. Specimens for TEM examination were prepared by carefully crushing the samples with a mortar and pestle set. The resulting powders were suspended in a volatile solvent and ultrasonicated to obtain a uniform suspension. One or two drops of this suspension were deposited onto a copper mesh grid coated with a holey carbon film (Quantifoil Micro Tools GmbH). The solvent was allowed to evaporate completely before examining the TEM specimens in a JEOL 2010 FasTEM operating at 200 kV. This instrument is equipped with a high-resolution objective lens pole-piece (spherical aberration coefficient Cs = 0.5mm) giving a point-to-point resolution of <0.19nm in phase contrast images. Bright field (BF) TEM images were acquired from these samples.

3. RESULTS

3.1. Cu precursor

The molecular structure of Cu precursor, CuDI6, was unambiguously established by single-crystal X-ray diffraction analysis and is shown in Figure 1. The following elemental percentages were found in the mass spectrum of CuDI6: C: 23.77%; H: 0.41%; F: 55.81%; Cu: 10.41%; N: 9.12%. These values are in very good agreement with calculated element percentages for $C_{12}H_4F_{18}CuN_4$;, C: 23.64%; H: 0.66%; F: 56.10%; Cu: 10.42%; N: 9.19%.

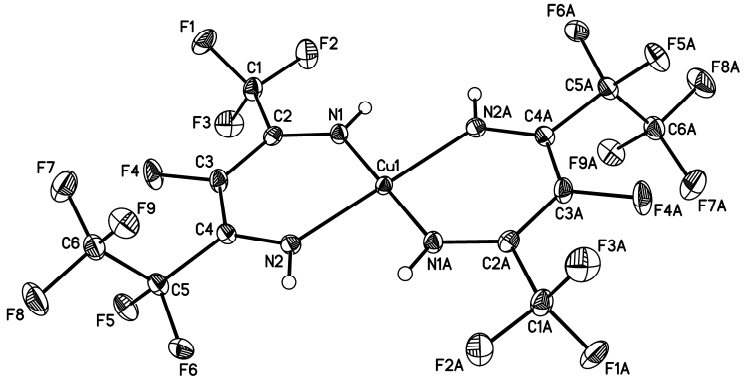

Figure 1 Molecular structure of CuDI6 (anisotropic displacement ellipsoids are drawn at 40% probability level).

3.2. Aerogel properties

The pore properties and the surface areas of the aerogels used in this study are given in the Table 2. All of the aerogels have relatively high surface areas varying between ~670-800 m^2/g. The aerogels do possess mesoporous structures given the average pore sizes of the aerogels. On the other hand, there is also evidence for the existence of some micropores. In this extent, the SA_{mic}/SA_{tot} ratio for CAs is higher than that of RFAs which is in agreement with the studies in the literature [20]. Correspondingly, although the S_{tot} of CA is higher than

that of the RFA, the values of their mesoporous area are close. The SA has relatively negligible microporous area as compared to the other aerogels.

Table 2 Pore properties of the aerogels used in SCD experiments

Aerogels	S_{tot} (m^2/g)	D (nm)	S_{mic} (m^2/g)	S_{tot}-S_{mic} (m^2)
CA	670	23.3	247	423
RFA	548	23.8	74	474
SA	793	20.6	11	782

S_{tot}: BET total surface area; D: BJH desorption pore diameter; S_{mic}: t-plot micropore area.

3.3. The adsorption isotherms

The adsorption isotherms for CuDI6 on CA, RFA and SA from $scCO_2$ at 10.6 MPa and 35 °C are presented in Figure 2. In all of the isotherms, the CuDI6 uptake increases non-linearly with increasing CuDI6 concentration in $scCO_2$. It is clear that at a particular CuDI6 concentration, the CA has the highest uptake and the SA has the lowest uptake. The isotherms are fitted well to Langmuir model which is given as

$$q = \frac{K_1 Q_0 C}{1 + K_1 C}$$

where q (mol/kg) is the uptake amount of the adsorbate (CuDI6) on RFA, K_1 (m^3 $scCO_2$/mol CuDI6) is the adsorption equilibrium constant, Q_0 is the uptake capacity (mole CuDI6/ kg aerogel) C is the CuDI6 concentration in $scCO_2$ (mol/ m^3 $scCO_2$) and the K_1Q_0 value is the relative affinity of CuDI6 towards the surface of adsorbent (aerogel). The corresponding Langmuir model parameters are given in Table 3. The aerogels' affinity for CuDI6 increases in the order CA>RFA>SA. The order of the affinity between the CuDI6 and aerogels arises due to the fact that, in the $scCO_2$ environment, hydrophobic CuDI6 partitions more to the hydrophobic CA than to the hydrophilic SA. On the other hand, all of the affinity values found in this work are lower than the values published before for the $Pt(cod)me_2$ adsorption on CAs [18] and RFAs [15] indicating weaker interaction of CuDI6 with the surface of aerogels as compared to $Pt(cod)me_2$. Relatively lower affinity values of CuDI6 with aerogels arise from the fact that it is a polyfluorinated compound and highly volatile. The uptake capacity of SA is the lowest one among other aerogels as shown in Table 3 even though its total surface area is the highest as shown in Table 2. The lowest uptake capacity of SA can be explained by its hydrophilic nature where adsorption sites available for such hydrophobic molecules are minimal. The relatively high CuDI6 uptake and capacity values of CA and RFA can also be explained in the same manner since these two aerogels are quite hydrophobic in nature. The capacity of CA and RFA was expected to be close even though the total surface area of CA is 18% more than that of the RFA. However, the S_{tot}-S_{mic} values that correspond to the mesoporous areas of both aerogels are quite close. As previously reported, the microporous area may or may not be available for the adsorption depending on the adsorbate molecular diameter [18, 21]. The molecular diameter of CuDI6 is 0.94 nm as calculated by the ArgusLab software and it is likely that the CuDI6 can not access to the adsorption sites in some micropores.

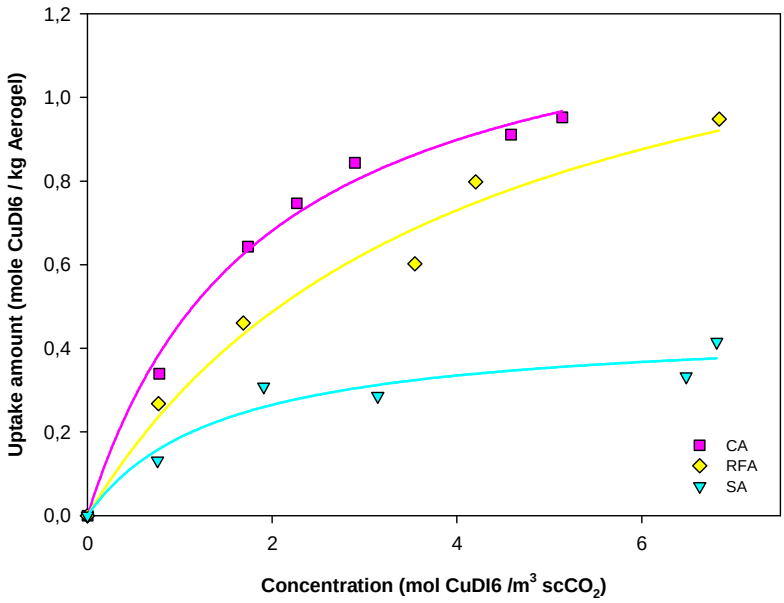

Figure 2 Adsorption isotherms of CuDI6-CO_2-aerogel systems at 10.6 MPa and 35°C (ρ_{CO2} = 736.1 kg/m^3)

.

Table 3 Langmuir isotherm parameters of the CuDI6-aerogel-$scCO_2$ systems (ρ_{CO2} = 736.1 kg/m^3)

Parameters	**CA**	**RFA**	**SA**
	35°C	**35°C**	**35°C**
Uptake capacity, Q_0 (mole adsorbate/ kg adsorbent)	1.320	1.483	0.455
Adsorption equilibrium constant, K_1 (m^3 $scCO_2$/ kg adsorbate)	0.534	0.244	0.695
Affinity, K_1Q_0 (m^3 $scCO_2$/ kg adsorbent)	0.705	0.361	0.225
R^2	0.994	0.990	0.993

3.4. Decomposition of adsorbed CuDI6

Aerogel-CuDI6 composites were exposed to Thermogravimetric analysis (TGA) in order to understand the decomposition characteristics of CuDI6. The TGA of neat and adsorbed CuDI6 is given in Figure 3. The neat CuDI6 lost its 74% of its weight at about 197 °C and at about 300 °C nearly 7% of the precursor remained. On the other hand, for the CuDI6 adsorbed on CA and SA, the weight loss was smaller than the neat one. At about 210°C, the weight loss was 51% and 69% for CA supported and SA supported CuDI6, respectively. These observations point out that CuDI6 decomposes on the surface of aerogels and does not evaporate.

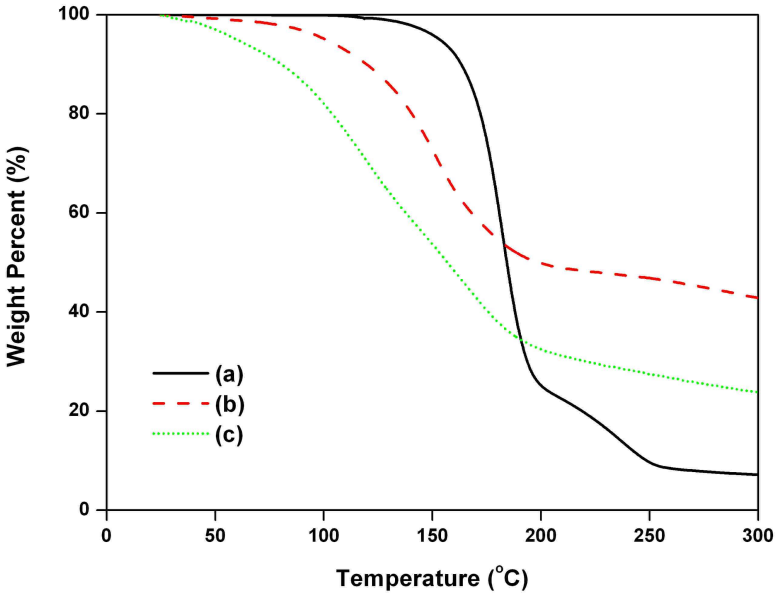

Figure 3 TGA of CuDI6 in N_2 flow with a heating rate of 10°C/min: (a) pure CuDI6; (b) adsorbed on CA; (c) adsorbed on SA; Curve (b) and (c) were plotted by subtracting the amount of aerogel.

3.5. Aerogel supported Cu nanostructures

We carried out a set of experiments where aerogel-CuDI6 composites were treated with H_2. Subsequently, we measured the XRD spectrum of the samples which are given in Figure 4. All of these samples possess approximately 4 wt. % of Cu. In Figure 4, the spectrum indicated the characteristic peaks of the metallic face-centered-cubic Cu, Cu_2O or CuO for different samples. The data in Figure 4 showed that utilization of various reaction media and different reaction temperatures resulted in Cu containing nanoparticles with various oxidation states. Characteristic peaks associated with CuO were observed after N_2 treatment at 300°C. Sample 6 which was treated in inert medium at 300°C. Since no H_2 was present in the medium, the reduction of copper to zero valence state did not occur. In the spectra shown in Figure 4.f where H_2 treatment was carried out subsequent to N_2 treatment at 300°C, Cu and Cu_2O peaks were obtained suggesting the chemical reduction of CuO. Interestingly, when the decomposition was carried out at 400°C in N_2 (Figure 4.g), Cu and Cu_2O phases appeared indicating a thermally induced reduction of CuO to Cu_2O and Cu. In the XRD spectra shown in Figure 4.c and d where only H_2 treatment was carried out Cu and Cu_2O peaks appeared. The Cu peak in Figure 4.b is very broad and overlaps with the broad peak of CA. Therefore, it was difficult to analyze this sample by XRD.

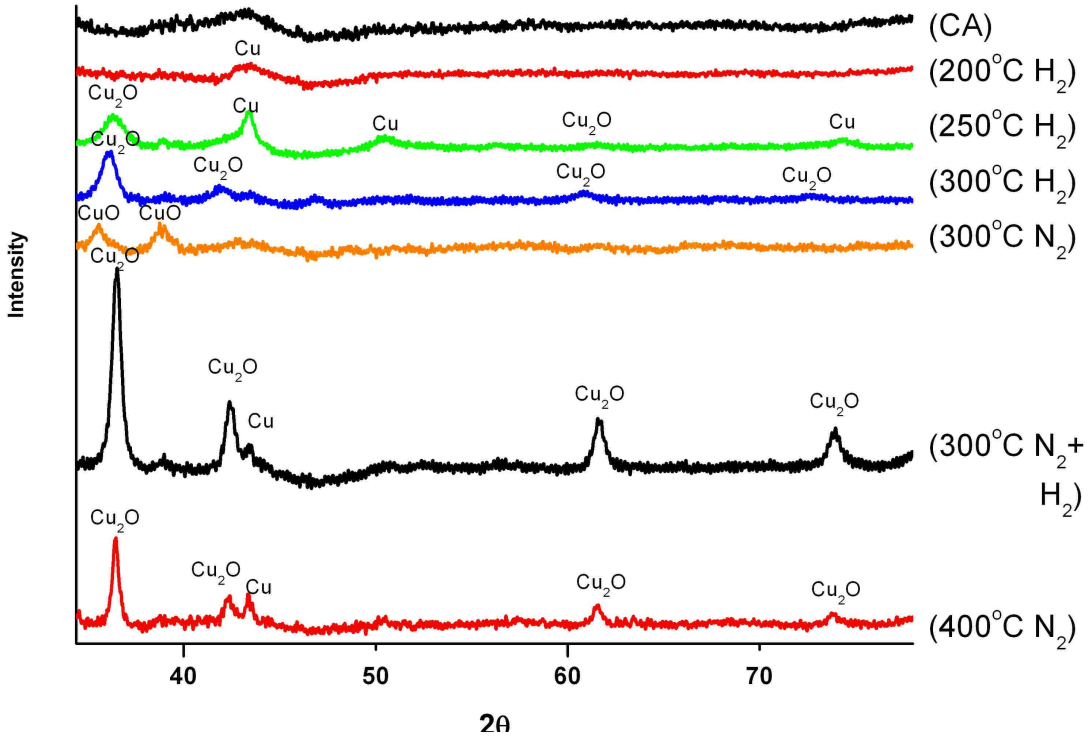

Figure 4 XRD spectra of the CA-Cu composites.

Figure 5 represents BF TEM images of CA-Cu composites. In these images, gray background is the CA and it is decorated with black dots which are the nanoparticles which are dispersed throughout the samples (Figure 5 a, c and e). TEM images shown in Figure 5.a & b were obtained from a sample which was first treated with O_2 at 160 °C and then with H_2 at 200 °C. The images showed a low concentration of particles with sizes around 40-50 nm.

Some images were taken using high magnification in order to characterize the chemical composition of the nanoparticles using lattice fringe analysis. As shown in Figure 5.c & d, nanoparticles with different lattice spacings were found. This sample was prepared with O_2 treatment at 160 °C then H_2 with 300 °C. When images such as Figure 5.d were analyzed, Cu nanoparticles with 1.808 Å lattice spacing associated with fcc (200) plane along with separate Cu_2O nanoparticles with 2.465 Å lattice spacing associated with Cu_2O (111) plane were observed. These spacings were either associated with Cu or Cu_2O indicating phase segregated nanoparticles. When the high magnification images of sample treated with H_2 at 250°C were analyzed, nanoparticles with core-shell morphologies were observed throughout the sample (Figure 5.e & f). As a result of the lattice spacing analysis, we concluded that the nanoparticles consisted of single crystal Cu in the core and Cu_2O in the shell. We suggest that as a result of the applied treatment, the adsorbed CuDI6 decomposed and as the ligands left the system as a gaseous mixture, the Cu nuclei were formed and then they grew to form nanoparticles. Subsequently, as the samples were contacted with air after the H_2 treatments, the surface of Cu nanoparticles were oxidized to give Cu_2O or CuO. However, the fact that previously mentioned various reaction configurations resulted in different nanostructures is interesting and the mechanism of these reactions merits further investigation.

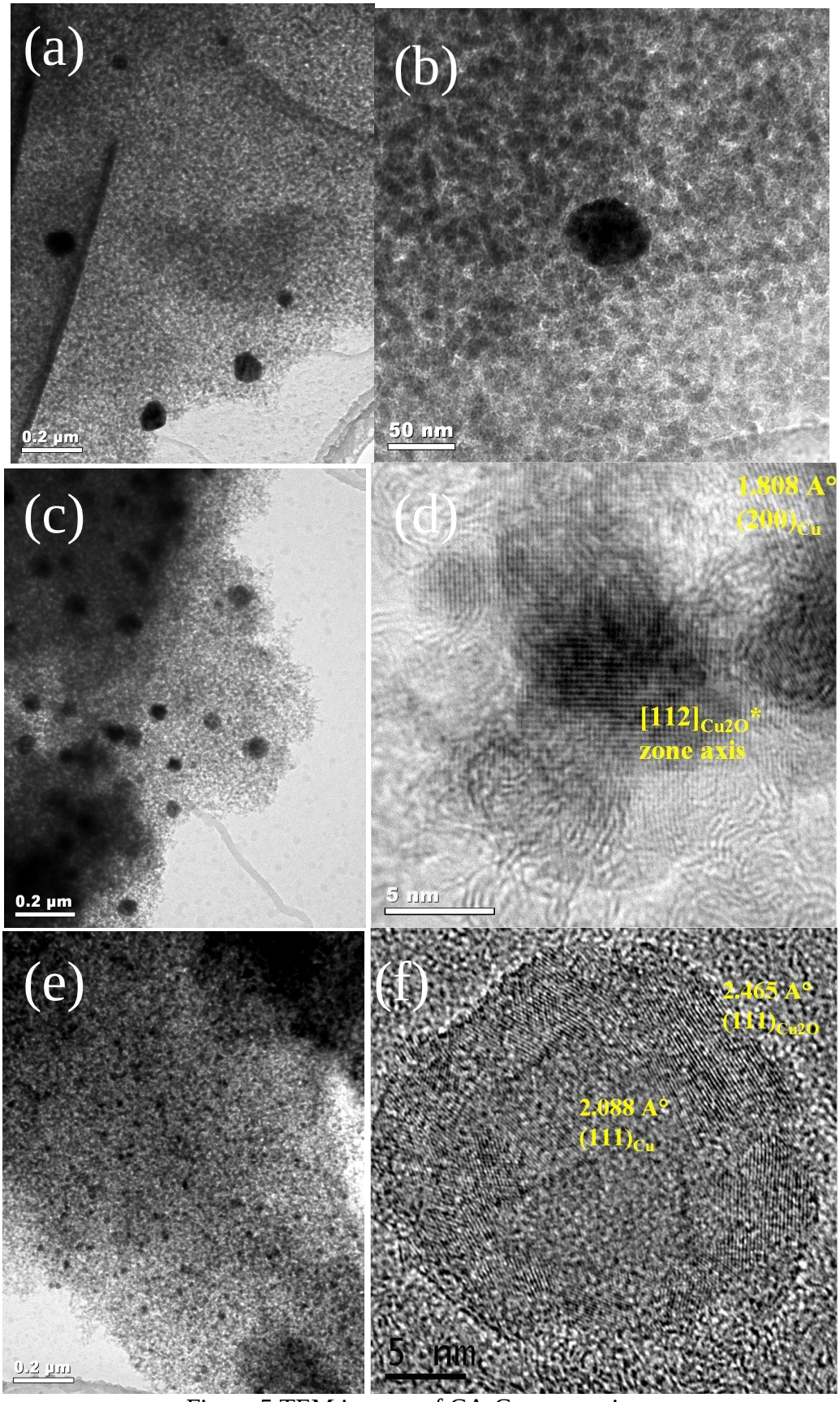

Figure 5 TEM images of CA-Cu composites.

4. CONCLUSION

Adsorption isotherms of CuDI6 on CA, RFA and SA were determined by analyzing the fluid phase concentrations in a batch system. Langmuir model fitted the experimental data very well. CuDI6 capacity of CA and RFA were found to be much higher than that of the SA.

When the CA-CuDI6 composites were treated with H_2 at 250°C, Cu@Cu_2O core-shell nanoparticles were formed whereas phase segregated Cu-Cu_2O nanoparticles were obtained when an O_2 treatment at 160 °C preceded the H_2 treatment at 300 °C. CuO nanoparticles were obtained after a N_2 treatment 300 °C.

REFERENCES

[1] G.H. Chan, J. Zhao, E.M. Hicks, G.C. Schatz, R.P. Van Duyne, Plasmonic Properties of Copper Nanoparticles Fabricated by Nanosphere Lithography, Nano Letters, 7 (2007) 1947-1952.

[2] Z. Liu, A. Wang, X. Wang, T. Zhang, Reduction of NO by Cu–carbon and Co–carbon xerogels, Carbon, 44 (2006) 2330–2356.

[3] J.H. Byeon, H.S. Yoon, K.Y. Yoon, S.K. Ryu, J. Hwang, Electroless copper deposition on a pitch-based activated carbon fiber and an application for NO removal, Surface & Coatings Technology, 202 (2008) 3571-3578.

[4] N. Muratova, Highly distributed copper nanoparticles on carbon supports for methanol steam reforming, in, Ruhr-Universität Bochum, Bochum, 2007.

[5] J.J. Watkins, T.J. McCarthy, Polymer/Metal Nanocomposite Synthesis In Supercritical CO2, Chemistry of Materials, 7 (1995) 1991-1994.

[6] Y. Zhang, C. Erkey, Preparation of supported metallic nanoparticles using supercritical fluids: A review, Journal of Supercritical Fluids, 38 (2006) 252-267.

[7] C. Erkey, Preparation of metallic supported nanoparticles and films using supercritical fluid deposition, Journal of Supercritical Fluids, 47 (2009) 517-522.

[8] S. Marre, A. Erriguible, A. Perdomo, F. Cansell, F. Marias, C. Aymonier, Kinetically Controlled Formation of Supported Nanoparticles in Low Temperature Supercritical Media for the Development of Advanced Nanostructured Materials, Journal of Physical Chemistry C, 113 (2009) 5096-5104.

[9] C. Aymonier, A. Denis, Y. Roig, M. Iturbe, E. Sellier, S. Marre, F. Cansell, J.L. Bobet, Supported metal NPs on magnesium using SCFs for hydrogen storage: Interface and interphase characterization, Journal of Supercritical Fluids, 53 (2010) 102-107.

[10] S.K. Morley, P. Licence, P.C. Marr, J.R. Hyde, P.D. Brown, R. Mokaya, Y. Xia, S.M. Howdle, Supercritical fluids: a route to palladium-aerogel nanocomposites, J. Mater. Chem. , 14 (2004) 1212.

[11] X.-R. Ye, Y. Lin, C. Wang, M.H. Engelhard, Y. Wang, C.M. Wai, Supercritical fluid synthesis and characterization of catalytic metal nanoparticles on carbon nanotubes, J. Mater. Chem., 14 (2004) 908.

[12] N.G. Smart, T. Carleson, T. Kast, A.A. Clifford, M.D. Burford, C.M. Wai, Solubility of chelating agents and metal-containing compounds in supercritical fluid carbon dioxide, Talanta, 44 (1997) 137-150.

[13] O. Aschenbrenner, S. Kemper, N. Dahmen, K. Schaber, E. Dinjus, Solubility of [beta]-diketonates, cyclopentadienyls, and cyclooctadiene complexes with various metals in supercritical carbon dioxide, The Journal of Supercritical Fluids, 41 (2007) 179-186.

[14] C.H. Yen, K. Shimizu, Y.Y. Lin, F. Bailey, I.F. Cheng, C.M. Wai, Chemical fluid deposition of pt-based bimetallic nanoparticles on multiwalled carbon nanotubes for direct methanol fuel cell application, Energy & Fuels, 21 (2007) 2268-2271.

[15] S.E. Bozbag, N.S. Yasar, L.C. Zhang, M. Aindow, C. Erkey, Adsorption of Pt(cod)me2 onto organic aerogels from supercritical solutions for the synthesis of supported platinum nanoparticles, The Journal of Supercritical Fluids, 56 (2011) 105–113.
[16] Y. Zhang, B. Cangul, Y. Garrabos, C. Erkey, Thermodynamics and kinetics of adsorption of bis(2,2,6,6-tetramethyl-3,5-heptanedionato) (1,5-cyclooctadiene) ruthenium(II) on carbon aerogel from supercritical CO2 solution, Journal of Supercritical Fluids, 44 (2008) 71-77.
[17] B. Cangul, L.C. Zhang, M. Aindow, C. Erkey, Preparation of carbon black supported Pd, Pt and Pd-Pt nanoparticles using supercritical CO2 deposition, Journal of Supercritical Fluids, 50 (2009) 82-90.
[18] C.D. Saquing, D. Kang, M. Aindow, C. Erkey, Investigation of the supercritical deposition of platinum nanoparticles into carbon aerogels, Microporous and Mesoporous Materials, 80 (2005) 11-23.
[19] R.W. Pekala, Organic aerogels from polycondensation of resorcinol with formaldehyde, Journal of Materials Science. , 24 (1989) 3221.
[20] H. Tamon, H. Ishizaka, M. Mikami, M. Okazaki, Porous Structure of Organic and Carbon Aerogels Synthesized by Sol-Gel Polycondensation of Resorcinol with Formaldehyde, Carbon, 35 (1997) 791-796.
[21] C.D. Saquing, T.T. Cheng, M. Aindow, C. Erkey, Preparation of platinum/carbon aerogel nanocomposites using a supercritical deposition method, Journal of Physical Chemistry B, 108 (2004) 7716-7722.